

Transient chaotic mixing during a baroclinic life cycle

J. von Hardenberg

Meteorologisches Institut der Universität Hamburg, Germany and Istituto di Cosmogeofisica, Torino, Italy

K. Fraedrich and F. Lunkeit

Meteorologisches Institut der Universität Hamburg, Germany

A. Provenzale^{a)}

Istituto di Cosmogeofisica, Torino, Italy

(Received 19 August 1999; accepted for publication 6 December 1999)

We discuss how atmospheric eddies affect transport and mixing of tracers at midlatitudes. To this purpose, we study baroclinic life cycles in a simple dynamical model of the atmosphere. We consider the trapping properties of the developing eddies and the characteristics of meridional transport, and we identify regions of increased mixing. Although the flow is in principle three-dimensional, we illustrate how some of the concepts developed in the study of two-dimensional chaotic advection provide useful information on tracer dynamics in more complicated flows. © 2000 American Institute of Physics. [S1054-1500(00)02401-0]

In many geophysical flows, coherent structures are a crucial component of the large and mesoscale dynamics. In particular, coherent eddies have been suggested to play a significant role in tracer transport both in the atmosphere and the oceans. Analogously, since midlatitude meridional transport is generally inhibited on a rotating sphere (due to local differential rotation), trapping and release of tracers by eddies may provide an important mechanism for meridional mixing in this type of flows. In the troposphere, baroclinic life cycles lead to the presence of strong transient eddies that can play the role of coherent structures. In this work we study the transient chaotic mixing induced by an individual baroclinic life cycle in a simple primitive equations model of a dry atmosphere.

I. INTRODUCTION

Tropospheric flows are very efficient in transporting Lagrangian tracers over large distances. This has important practical consequences, such as global dispersion of pollutants and greenhouse gases. In order to obtain a theoretical understanding of tropospheric transport, one needs to identify the individual processes that are responsible for the various facets of the problem. In this spirit, Knobloch & Weiss (1987) and Pierrehumbert (1991) considered the mixing properties of modulated traveling waves, and Pierrehumbert & Yang (1993) discussed the role of chaotic advection on isentropic surfaces in a simple general circulation model of the atmosphere. More recently, Bowman & Cohen (1997) considered the mechanisms leading to homogenization in a 2D (two-dimensional) vertical, zonally averaged, slice of the atmosphere, Stone *et al.* (1998) studied transport of passive tracers in baroclinic wave life cycles, and Methven & Hoskins (1999) studied tracer dynamics in low-resolution wind fields by contour advection techniques.

Among the basic mechanisms that control tropospheric transport, the role played by transient baroclinic eddies deserves particular attention and has still to be fully clarified. In the troposphere, these structures form strong potential vorticity (PV) anomalies that carry a significant fraction of the transient kinetic energy of midlatitude atmospheric flows. Although their lifetime is shorter than that of quasigeostrophic eddies [see, e.g., Provenzale (1999)], it is tempting to consider these atmospheric eddies as the “coherent structures” of midlatitude tropospheric flows.

In past studies, the effects of coherent vortices on particle transport have been studied mainly in barotropic conditions. In two-dimensional turbulence, coherent structures such as vortices and jets represent strong transport barriers that trap tracers for long times and strongly affect the overall mixing properties of the system [Elhmaïdi *et al.* (1993); Babiano *et al.* (1994); Weiss *et al.* (1998); Provenzale 1999)]. Also, while in the chaotic background small patches of tracers are quickly stretched and folded by chaotic advection, leading to fast mixing, the interior of barotropic vortices represent an island of regular motion [Babiano *et al.* (1994), Kuznetsov & Zaslavsky (1998)]. Here, mixing happens only on diffusive time scales, consistent with the analysis by Rhines & Young (1983) on the effect of closed potential vorticity isolines on tracer mixing.

Two-dimensional turbulence, however, is not a very realistic model of the complex dynamics of tropospheric flows. Even in the simple quasi-geostrophic approximation (e.g., Pedlosky 1987), baroclinic effects are crucial as the eddies develop from baroclinic instability of the basic flow. In this work, we apply the approach developed in the study of two-dimensional chaotic advection to the exploration of the transport properties of atmospheric baroclinic eddies, and we show that some of the concepts developed in simpler situations are useful also in this case.

As a minimal model to study this issue, here we concentrate on the properties of transient chaotic mixing induced by a single baroclinic life cycle in a primitive equations model

^{a)}Electronic mail: anto@icg.to.infn.it

of the atmosphere. This type of dynamics is richer than that of quasigeostrophic flows, allowing for ageostrophic effects and three-dimensional motion, even though the resolution used here does not allow for fully resolving the behavior of frontal regions that can indeed play an important role in the real atmosphere. In addition, the model considered here does not contain water vapor, and diabatic effects are thus limited. Without moisture, in fact, there is little cross-isentropic mixing, and particles do not disperse much from an isentropic surface. Notwithstanding these shortcomings, we see this study as an intermediate step toward extending the concepts developed in the study of chaotic advection to more realistic geophysical flows.

II. A SIMPLIFIED GCM

The Eulerian flow model used in this study is a simplified general circulation model of the atmosphere (SGCM) that solves the primitive equations for a dry atmosphere on the spherical domain. Despite its simplicity, the model discussed here is able to satisfactorily reproduce the large scale features of planetary atmospheric circulations. Named PUMA (Portable University Model of the Atmosphere), it represents a refinement of the model introduced by James & Gray (1986), based on the multi layer spectral model by Hoskins & Simmons (1975). Further details and discussions are given by Blackburn (1985), James & Dodd (1993), Friis *et al.* 1998, and Fraedrich *et al.* (1998).

In the PUMA model, the momentum equations are formulated in terms of the vertical component of absolute vorticity ζ and horizontal divergence D , using σ coordinates on the vertical ($\sigma = p/p_s$ where p is pressure and p_s is surface pressure). The vertical velocity in physical coordinates can be obtained from the other dynamical variables as indicated by Hoskins & Simmons (1975). Temperature is expressed as $T = \bar{T}(\sigma) + T'$ where T' is the fluctuating component. Continuity is expressed as a prognostic equation for p_s . The model equations are written as:

$$\frac{\partial \zeta}{\partial t} = \frac{1}{1-\mu^2} \frac{\partial}{\partial \lambda} \mathcal{F}_v - \frac{\partial}{\partial \mu} \mathcal{F}_u - \frac{\zeta - \mu}{\tau_D} + K(-1)^{p-1} \nabla^{2p} (\zeta - \mu), \quad (1)$$

$$\frac{\partial D}{\partial t} = \frac{1}{1-\mu^2} \frac{\partial}{\partial \lambda} \mathcal{F}_u + \frac{\partial}{\partial \mu} \mathcal{F}_v - \nabla^2 \left(\frac{U^2 + V^2}{2(1-\mu^2)} + \Phi + \bar{T} \ln p_s \right) - \frac{D}{\tau_D} + K(-1)^{p-1} \nabla^{2p} D, \quad (2)$$

$$\frac{\partial T'}{\partial t} = - \frac{1}{1-\mu^2} \frac{\partial}{\partial \lambda} (UT') - \frac{\partial}{\partial \mu} (VT') + DT' - \dot{\sigma} \frac{\partial T}{\partial \sigma} + \kappa \frac{T\omega}{p} + \frac{T_E - T}{\tau_E} + K(-1)^{p-1} \nabla^{2p} T', \quad (3)$$

$$\frac{\partial \ln p_s}{\partial t} = - \frac{U}{1-\mu^2} \frac{\partial}{\partial \lambda} \ln p_s - V \frac{\partial}{\partial \mu} \ln p_s - D - \frac{\partial \dot{\sigma}}{\partial \sigma}, \quad (4)$$

$$\frac{\partial \Phi}{\partial \ln \sigma} = -T, \quad (5)$$

where λ and ϕ are longitude and latitude respectively, $\mu = \sin \phi$, Φ is the geopotential, κ is the adiabatic coefficient and ω is vertical velocity. We also use the abbreviations $U = u \cos \phi = u \sqrt{1-\mu^2}$ and $V = v \cos \phi = v \sqrt{1-\mu^2}$, $\mathcal{F}_u = V\zeta - \dot{\sigma}(\partial U/\partial \sigma) - T'(\partial \ln p_s/\partial \lambda)$ and $\mathcal{F}_v = -U\zeta - \dot{\sigma}(\partial V/\partial \sigma) - T'(1-\mu^2)(\partial \ln p_s/\partial \mu)$.

Equations (1) and (2) are the vorticity and divergence equations, respectively, Eq. (3) is the thermodynamic equation, Eq. (4) is the conservation of mass (continuity), and Eq. (5) expresses hydrostatic equilibrium in σ coordinates. An hyperviscous dissipation, $K(-1)^{p-1} \nabla^{2p}$, is used in Eqs. (1)–(3) to parametrize subgrid-scale turbulent dissipation. The linear Rayleigh friction terms, $-(\zeta - \mu)/\tau_D$ and $-D/\tau_D$ in Eqs. (1) and (2), respectively, are used to parametrize surface drag. The relaxation time scale τ_D is set to its maximum value at the surface and it decreases to zero with growing pressure height. The thermodynamic equation [Eq. (3)] contains a linear Newtonian cooling term, $(T_E - T)/\tau_E$, that is used to parametrize diabatic processes. Due to this term, the model temperature relaxes to a fixed pole-equator temperature gradient T_E , which is balanced by thermal wind and provides the potential energy for baroclinic instability.

The numerical model used in this work is pseudospectral in the horizontal, as it solves the linear terms in spectral space and the nonlinear terms on a fixed Gaussian grid [Orszag 1970]. Any generic dynamical variable S is represented by a truncated series of spectral harmonics $S(\lambda, \mu) = \sum_{n,m} S_n^m P_n^m(\mu) e^{im\lambda}$, where $P_n^m(\mu)$ are the associated Legendre functions. The truncation employed here is a triangular scheme with $n \geq m$. A fast Fourier transform is used in the zonal direction, giving the half transforms $S^m(\mu)$. The spectral coefficients are then obtained integrating with respect to μ , $S_n^m = \int_{-1}^1 S^m(\mu) P_n^m(\mu) d\mu$. Finite differences are used in the vertical, with the prognostic variables ζ , D , T' defined on σ levels, and the vertical velocities $\dot{\sigma}$ defined halfway between the levels. Vertical velocities vanish on $\sigma=0$ and $\sigma=1$. The time-stepping is semi-implicit and uses a filter proposed by Robert (1966). In the following simulations, we use a T42 resolution in the horizontal, corresponding to 128×64 Gaussian grid points, and 10 σ levels in the vertical. The time step is set to $\Delta t = 30$ min.

The Lagrangian dynamics of this flow is studied by three-dimensional advection of neutrally buoyant, passive tracer particles. In spherical coordinates, the advection of an individual tracer particle may be expressed as

$$\frac{d\lambda}{dt} = \frac{u(\lambda, \phi, t)}{R \cdot \cos \phi}, \quad \frac{d\phi}{dt} = \frac{v(\lambda, \phi, t)}{R}, \quad \frac{d\xi}{dt} = \omega, \quad (6)$$

where R is the radius of the sphere, (λ, ϕ) are the zonal and meridional positions of the advected particle, ξ is its vertical position in σ coordinates, u and v are the zonal and meridional Eulerian velocities, respectively, and ω is the vertical velocity in σ coordinates.

Time integration of the tracer trajectories is based on a leap-frog scheme with periodic Adams–Moulton correction steps to damp the computational mode. This scheme allows

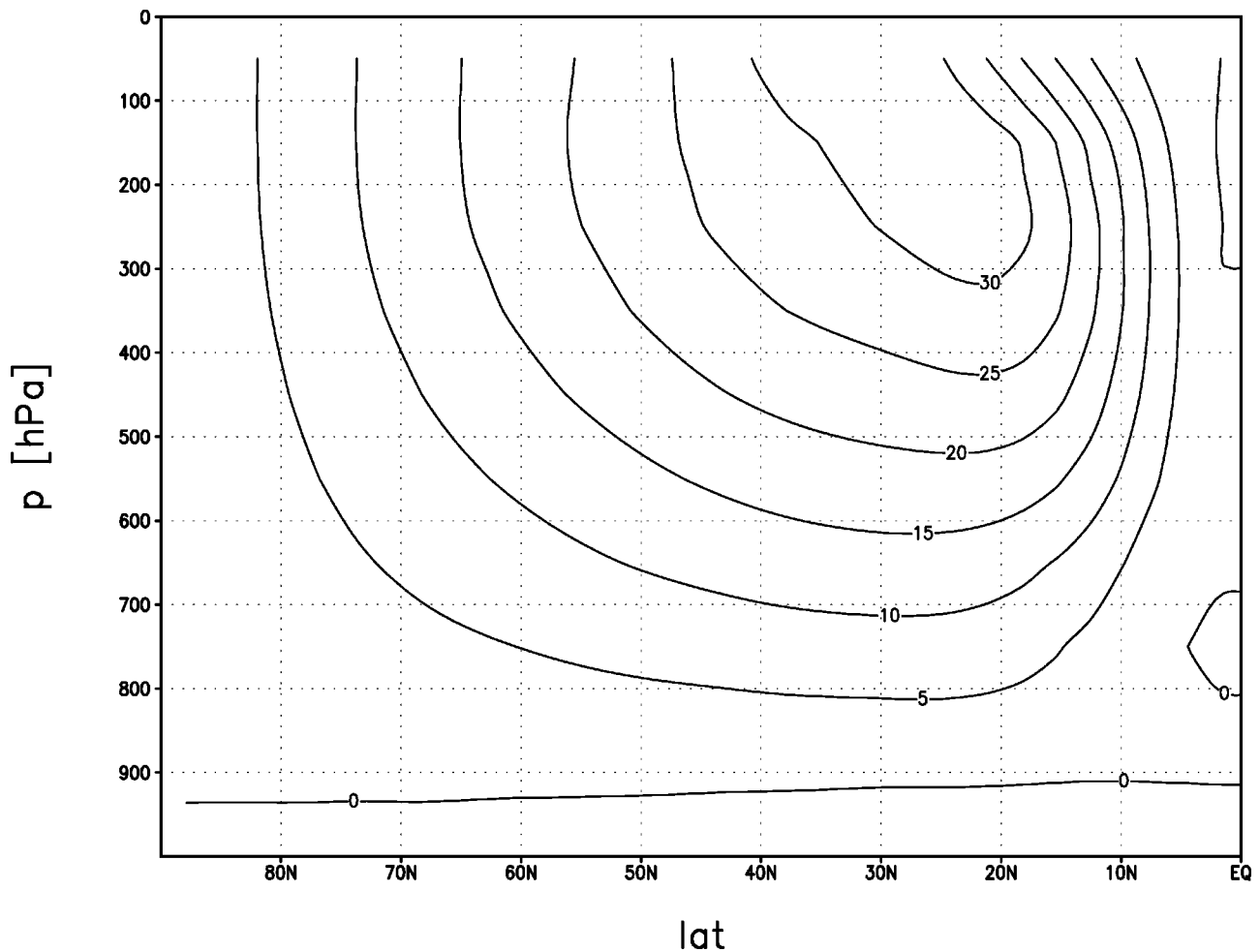


FIG. 1. Zonally averaged wind speed [in m/s], used as a basic state upon which initial perturbations are imposed.

for a greater accuracy and it is less dissipative than the implicit time stepping scheme used for the Eulerian fields. The zonal and meridional wind velocities u and v and the vertical tendency ω provided by the Eulerian field on a Gaussian grid at different model levels are interpolated to the tracer positions (λ, ϕ, ξ) using linear interpolation.

III. BAROCLINIC LIFE CYCLES

The linear theory of baroclinic instability represents a simple framework where to study the birth and initial development of transient atmospheric eddies. More than twenty years ago, Simmons & Hoskins (1976a), (1976b), (1978) showed that there is good agreement between the mechanism of baroclinic instability in primitive equation models and the behavior of real atmosphere. Since then, the life cycles of nonlinear baroclinic waves have been intensively studied [Simmons & Hoskins (1980); Gutowski *et al.* (1989), (1992); Branscome *et al.* (1989); Barnes & Young (1992); Thorncroft *et al.* (1993); Lee & Feldstein (1996); Stone *et al.* (1998)]. In particular, Thorncroft *et al.* (1993) have identified two different paradigms of life cycle evolution [originally denoted the “basic” and “anomalous” cases by Simmons & Hoskins (1980)], and Stone *et al.* (1998) have explored the transport properties of these two types of life cycles.

A simple way to generate a baroclinic life cycle is to introduce a small perturbation in one or more of the dynamical fields, starting from an appropriate baroclinic, zonally symmetric state. Through baroclinic instability, the available potential energy is transformed into eddy kinetic energy. The perturbation grows exponentially and eventually starts releasing its eddy kinetic energy to the mean flow by barotropic decay.

The choice of the basic state to use is not completely straightforward. A first possibility is to use a climatic average (zonal and time average) of the dynamical fields obtained by a long-time integration of the primitive equations. A clear advantage of this approach is that the initial state resembles what we would expect to be a “reasonable” atmosphere. However, the drawback is that, due to the nonlinear terms in the primitive equations, this state is not necessarily a stationary solution of the equations of motion. The possible nonstationarity of the basic state, then, makes it difficult to identify the effects due to the baroclinic life cycle itself.

Another option, and the one used by Simmons & Hoskins, is to define an initial zonal wind profile obtained, e.g., from real data, and to determine the corresponding temperature profile that satisfies thermal wind balance. This allows for studying different initial zonal mean states, but it can

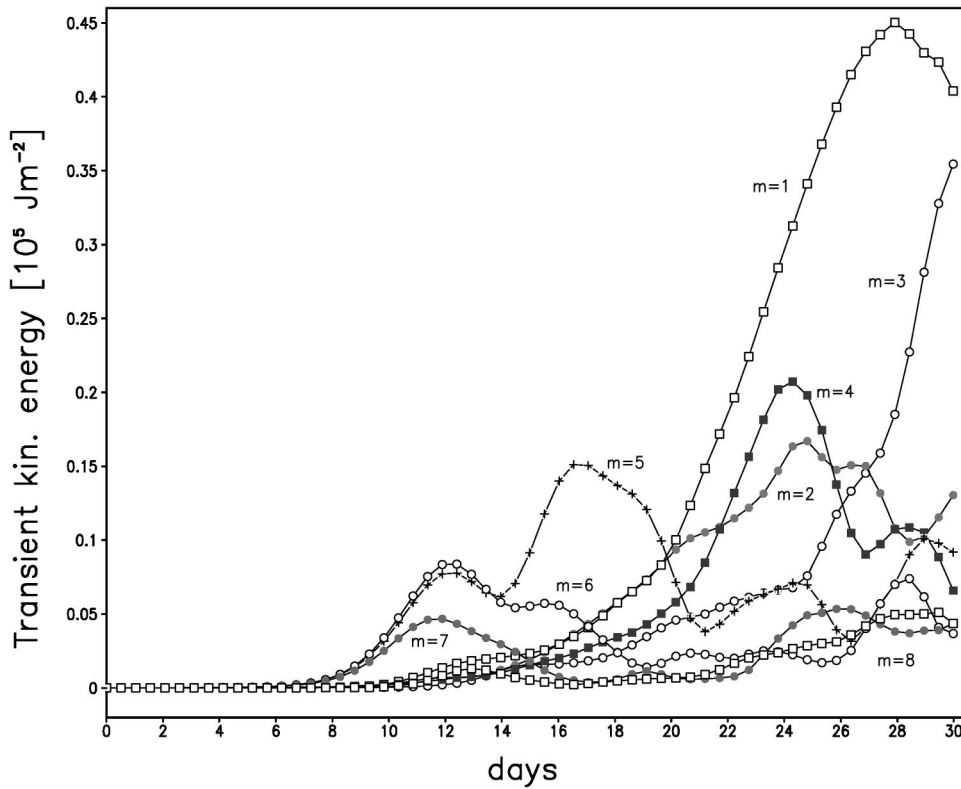


FIG. 2. Time evolution of the transient eddy kinetic energy for different zonal modes.

impose a particularly complicated temperature profile to the model.

In the present work, we prefer to keep a simple relaxation temperature profile and use as initial state the solution reached by the model after turning off zonal variability (i.e., by setting to zero all zonal spectral components with $m \neq 0$ for all dynamical variables). Under these conditions, the model reaches a stationary state that depends only on the (fixed) meridional and vertical temperature profiles imposed to the system, with thermal winds in geostrophic balance with the temperature gradient. Figure 1 shows a meridional section of the initial state (zonal wind profiles) obtained with this approach. This state possesses an Hadley circulation (Held & Hou 1980) and it is characterized by a jet heavily shifted southward and strong baroclinicity. These latter properties are associated with winter conditions.

The standard technique to perturb the basic state, as discussed by Simmons & Hoskins (1976a), (1976b), (1980) and Pierrehumbert (1995), uses the fastest linear growing mode as an initial perturbation. Figure 2 shows the evolution of the kinetic energy associated with different zonal perturbation modes. The mode with $m=7$ is one of the fastest growing modes for the basic state chosen here, consistent with the results of Simmons & Hoskins (1976a), (1976b), who found the $m=6,7$ modes to be among the fastest growing ones for the basic state they considered. Thus, in the following we perturb our basic state with a small $m=7$ perturbation.

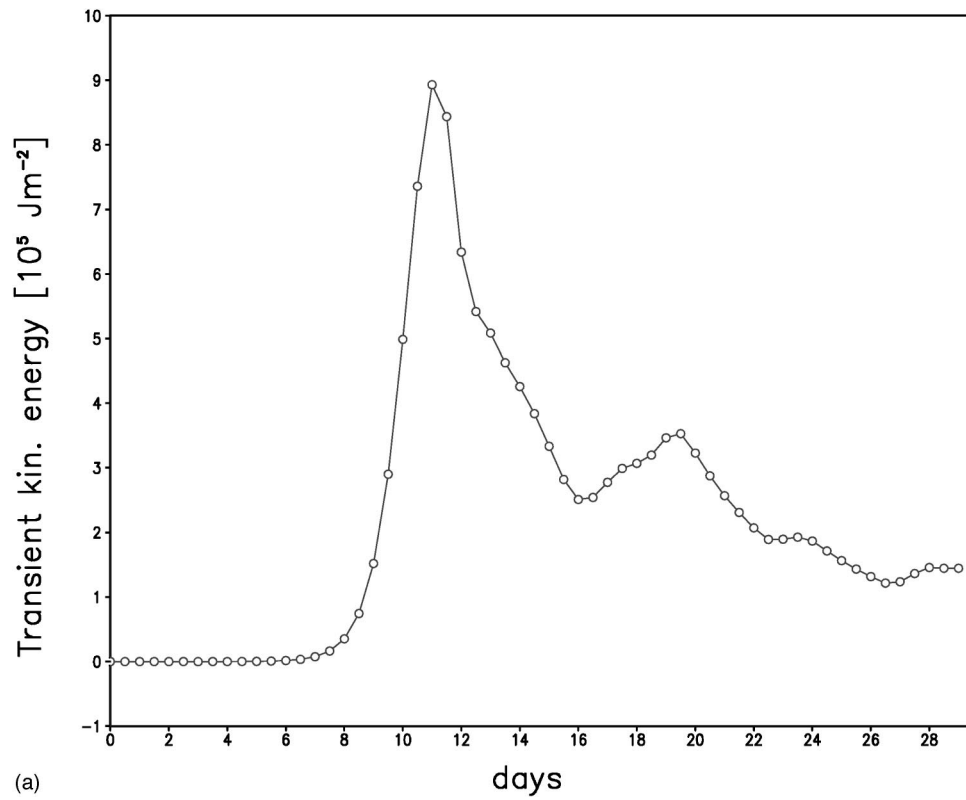
The net effect of a baroclinic life cycle is a conversion of zonal available potential energy into zonal kinetic energy, i.e., an increase of the zonal mean flow. This energy is then dissipated mainly by large scale friction. Thus, after one life cycle the zonal mean flow becomes more energetic and the

initial basic state changes. In the following, we switch off Newtonian cooling and Rayleigh friction during the evolution of the life cycle, allowing for just one full cycle and avoiding a cascade of successive secondary life cycles. The only diabatic effect remaining is diffusion. Figure 3(a) shows the time evolution of the transient kinetic energy during the baroclinic life cycle, and Fig. 3(b) shows the energy conversion terms. Despite the different form of perturbation and the different basic state chosen here, the similarity between these energy curves and those obtained by Simmons & Hoskins (1976a), (1976b), (1980) is striking.

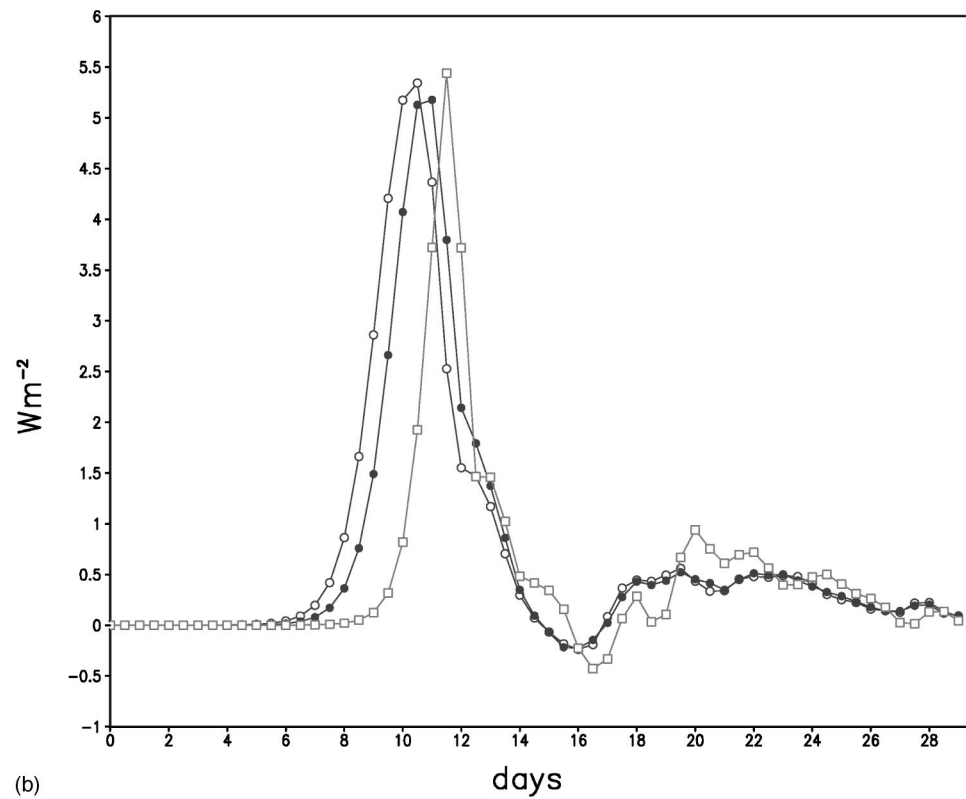
Figure 4 shows the development of the cyclonic eddy, as seen on the 315 °K isentrope, in various phases of the life cycle. Upper panels show potential vorticity (PV) and lower panels show relative vorticity. The times shown in this figure correspond respectively to eddy kinetic energy starting to grow sensibly ($t=9.5$ days), reaching a maximum ($t=11.5$ days), decreasing again (when barotropic energy transfer to zonal mean flow starts to operate, $t=13.5$ days) and reaching a final plateau, when the energy conversion terms vanish ($t=15.5$ days). The second half of the life cycle corresponds to tilting and shearing of the eddy, that decays barotropically. Note, also, that a cutoff region of stratospheric air is formed. This cutoff region survives for a long time after the end of the life cycle and it plays an important role in the Lagrangian dynamics, as we show below.

IV. TRACER DYNAMICS IN TRANSIENT EDDIES

Coherent barotropic vortices trap particles for long times [e.g., Provenzale (1999)], inducing characteristic signatures on particle transport. Tropospheric eddies, however, are rela-



(a)



(b)

FIG. 3. (a) Time evolution of the global transient kinetic energy during the baroclinic life cycle. (b) Time evolution of the energy conversion terms: Open circles indicate conversion from zonal potential energy to eddy potential energy; filled circles refer to conversion from eddy potential energy to eddy kinetic energy; open squares refer to conversion from eddy kinetic energy to zonal kinetic energy.

tively short lived with respect to their typical eddy turnover time. Moreover, they are strongly sheared during their evolution and do not always possess closed PV isolines at all heights. As such, they do not completely fit in the definition

of “coherent structures” [e.g., Lesieur (1990)] and it is not clear whether they are able to trap tracers, at least temporarily.

In order to address this issue, we have seeded 4096 trac-

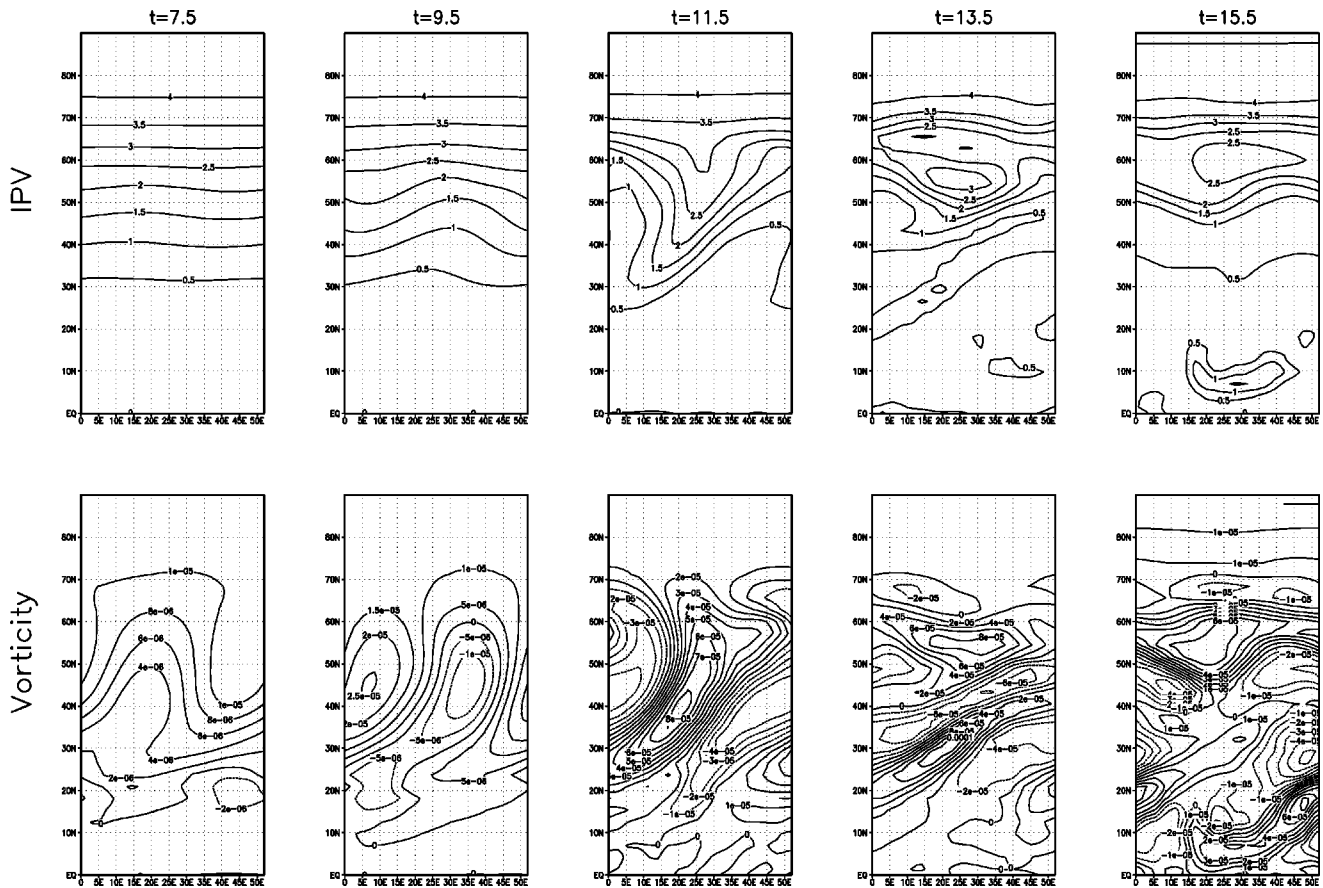


FIG. 4. Maps of potential vorticity in Potential Vorticity Units (upper panels) and of relative vorticity in [1/s] (lower panels) during the life cycle evolution, on the 315 °K isentrope. Time in days from the beginning of the evolution is indicated in the figure.

ers in circular patches of radius $r=2^\circ$, at times $t=9.5, 11.5, 13.5$ days, on the 315 °K isentrope. Tracers are seeded both inside and outside the eddy, as defined by relative vorticity isolines at $t=9.5$ and by PV isolines at $t=11.5, 13.5$ days. Figure 5 shows the tracer positions at the beginning and after 8 days of evolution, superposed to the corresponding PV isolines.

At $t=9.5$, the initial positions of the two tracer distributions correspond respectively to the relative vorticity minimum at ($35^\circ\text{E}, 45^\circ\text{N}$) and the high shear region at ($20^\circ\text{E}, 45^\circ\text{N}$). After 8 days, both distributions are stretched and folded by chaotic advection and they have undergone strong mixing. No trapping has occurred.

At $t=11.5$, the initial positions are at ($25^\circ\text{E}, 60^\circ\text{N}$) and ($45^\circ\text{E}, 60^\circ\text{N}$), corresponding, respectively, to the area where the cut-off region is developing and to a high shear region. The first distribution, even if elongated, is captured by the cut-off region, whereas the second tracer distribution undergoes chaotic stretching and folding.

Finally, at time $t=13.5$ days, we seed tracers at ($25^\circ\text{E}, 55^\circ\text{N}$) and ($45^\circ\text{E}, 55^\circ\text{N}$), again corresponding to the cut-off region and to a high-shear area. We observe particle trapping by the cut-off region and strong mixing in the highly sheared region.

These results indicate that the only trapping taking place during a baroclinic life cycle is associated with the cutoff region of stratospheric air, which represents the only true

coherent structure with closed vorticity isolines of the flow studied here. Once more, long-lived closed vorticity isolines show to be the main reason why tracer trapping can occur [Rhines & Young (1983)].

V. WHERE DOES THE FLUID GO TO?

A localized concentration of tracers is stretched and stirred by the flow evolution. During this process, initially close particles can separate exponentially fast from each other, and individual particles reach locations that can be quite far from their initial position. Some of these effects are quantified by evaluating the Lagrangian Lyapunov exponents of the flow, and by estimating the behavior of relative and absolute dispersion. All these measures refer to the “future” of a tracer distribution, and provide information on how a patch of tracers will move and stretch during the flow evolution.

A. Finite-time Lyapunov exponents

Useful statistics to quantify pair separation and stretching are the finite-time Lyapunov exponents (or “local” Lyapunov exponents). These were introduced by Lorenz (1965) to quantify predictability of weather patterns and have been proposed as means to identify mixing regions in inhomogeneous atmospheric fields [Pierrehumbert (1991); Pierrehumbert & Yang (1993)]. In this approach, for each

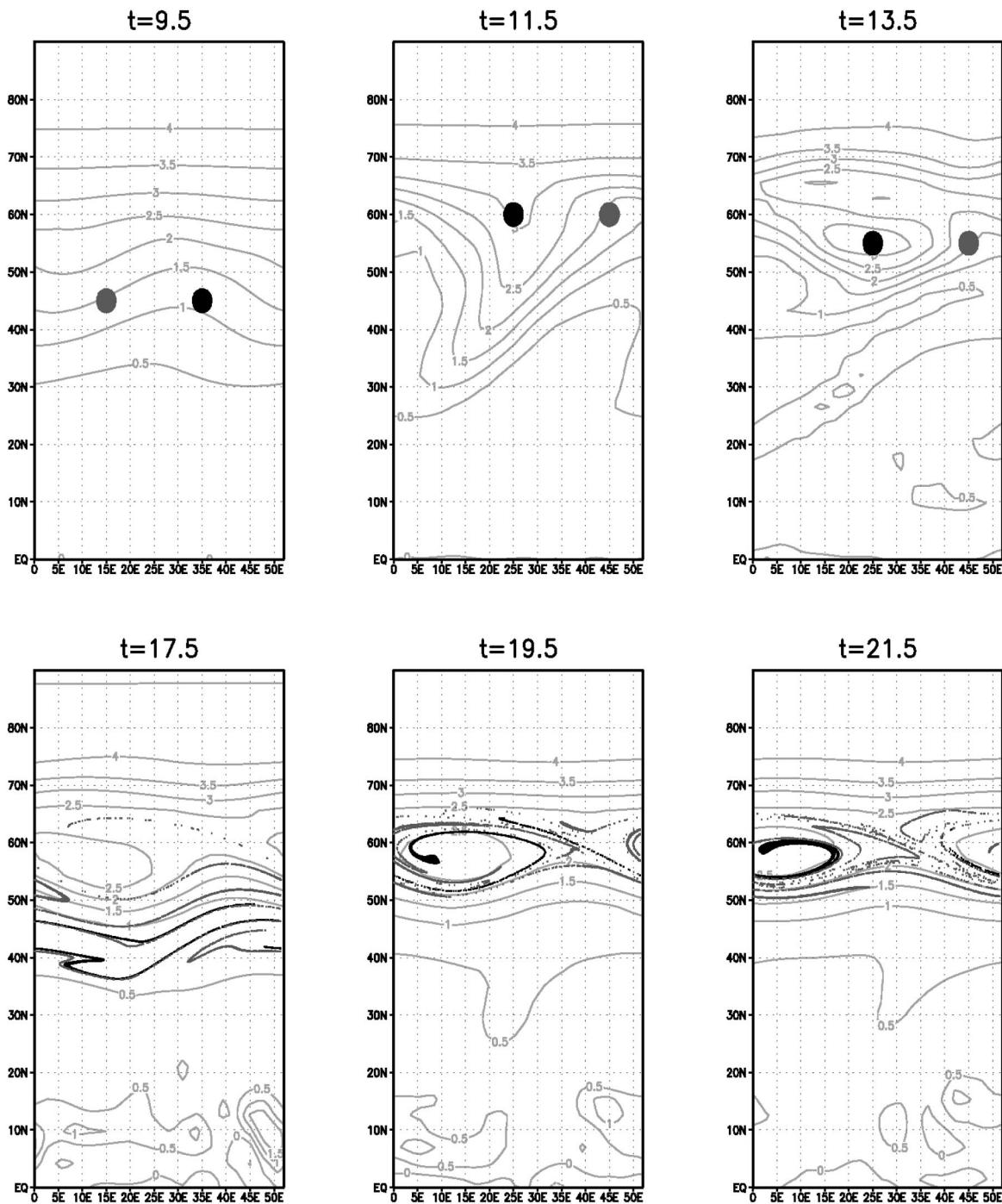


FIG. 5. Positions of the tracers seeded in two initial patches at times $t=9.5, 11.5, 13.5$ days (upper panels). Isolines indicate isentropic potential vorticity in PVU. The tracer evolution has been followed for 8 days; lower panels show the final positions of the tracers.

particular initial tracer position one evaluates the local linearized stretching rates along the particle trajectory, and average them over a fixed (and usually small) time T . The maximum growth rate evaluated in this way provides an estimate of the maximum local Lyapunov exponent Λ_T . Clearly, Λ_T depends on the initial tracer position. In the limit for $T \rightarrow \infty$, Λ_T converges to the maximum Lagrangian Lyapunov exponent for the selected initial position. For ergodic systems, the Lagrangian Lyapunov exponents are independent of the initial particle position.

To obtain an Eulerian map of the maximum finite-time

Lyapunov exponent as a function of the initial tracer position, we sample the physical domain on a regular grid, obtaining a field of local Lyapunov exponents $\Lambda_T(\lambda, \phi)$. The possible relationships of this quantity with other Eulerian dynamical fields (e.g., kinetic energy, vorticity) can then be analyzed. In the following, we calculate the maximum local Lyapunov exponent following Pierrehumbert & Yang (1993). We calculate the eigenvectors and eigenvalues of the horizontal velocity Jacobian along a particle trajectory, and average them over the portion of trajectory we consider. Although tracer advection is fully three-dimensional, in the cal-

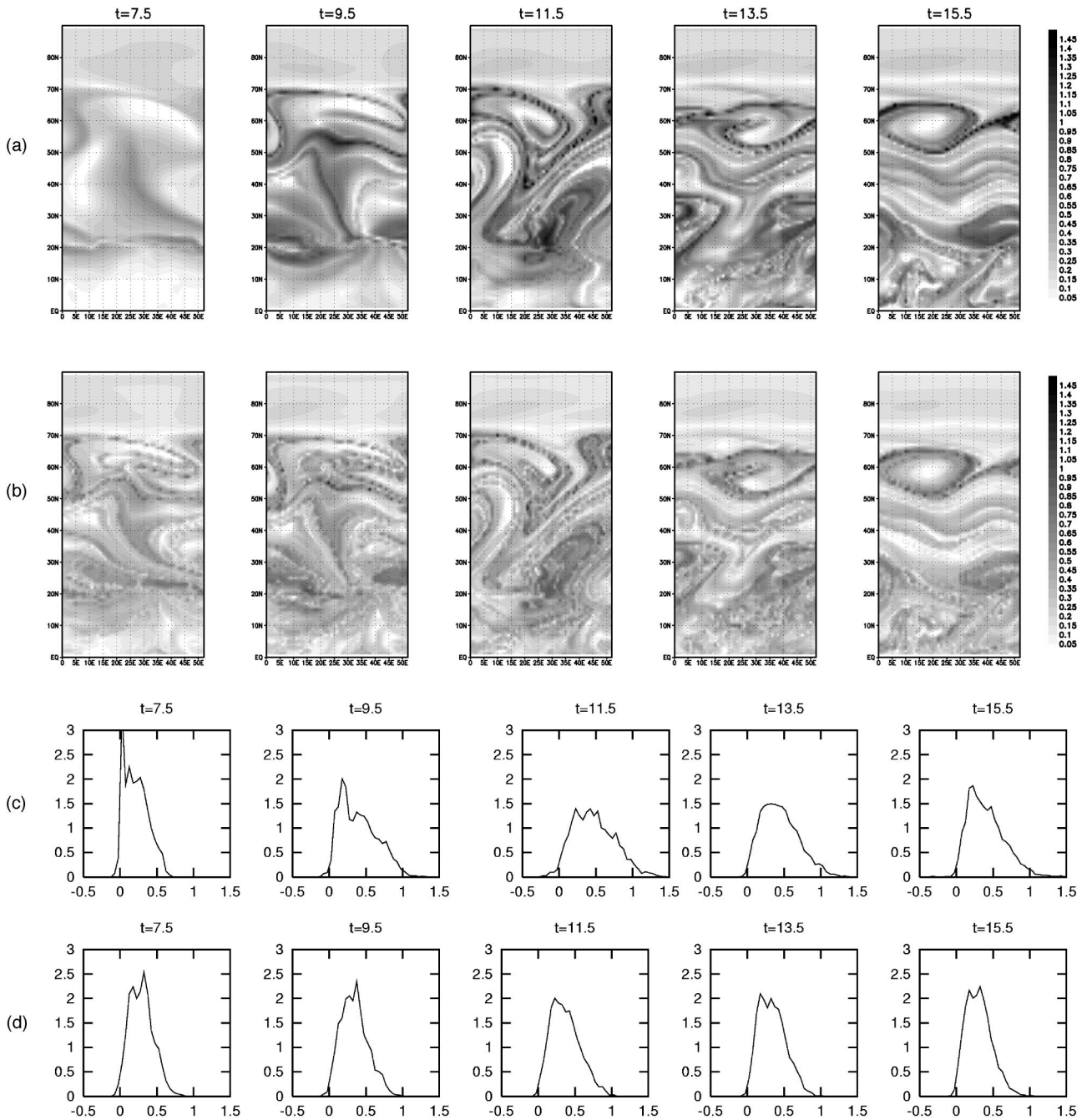


FIG. 6. Finite-time Lyapunov exponents at different evolute stages of the life cycle, with seeding on the 315 °K isentrope. Panels (a) show the maps of finite-time maximum Lyapunov exponent for a five-day integration and panels (b) for a 10 day integration. Panels (c) and (d) show the probability distribution of the finite-time maximum Lyapunov exponents for the two integration times.

culuation of Lyapunov exponents we estimate only horizontal stretching. This is the dominant mechanism for the model used here, on the short time span we are interested in.

Figures 6(a) and 6(b) show maps of maximum finite-time Lyapunov exponent, Λ_T , obtained by seeding tracers on a regular grid with mesh size $\Delta=1^\circ$, in the Northern hemisphere between 0 and 52 °E [recall that the Eulerian field is zonally periodic with symmetry $m=7$]. The corresponding probability distributions of maximum finite-time Lyapunov exponents for integration of 5 or 10 days are shown in Figs.6(c) and 6(d).

Figure 6(a) and 6(b) indicate that the developing eddy

cannot be associated with a region of small Lyapunov exponents. Only the final cutoff region displays low values of Λ_T in its interior, indicating that this is a region of quasi-regular Lagrangian motion, analogously to what has been observed for barotropic vortices [Babiano *et al.* (1994); Provenzale (1999)]. High values of Λ_T are found in the shear-dominated region at the edge of the cut-off region, again similarly to what happens for coherent barotropic vortices.

Finally, the distributions shown in Figs. 6(c) and 6(d) agree with those found by Pierrehumbert & Yang (1993), displaying a tendency towards becoming progressively narrower as the integration time T increases. Also in our case,

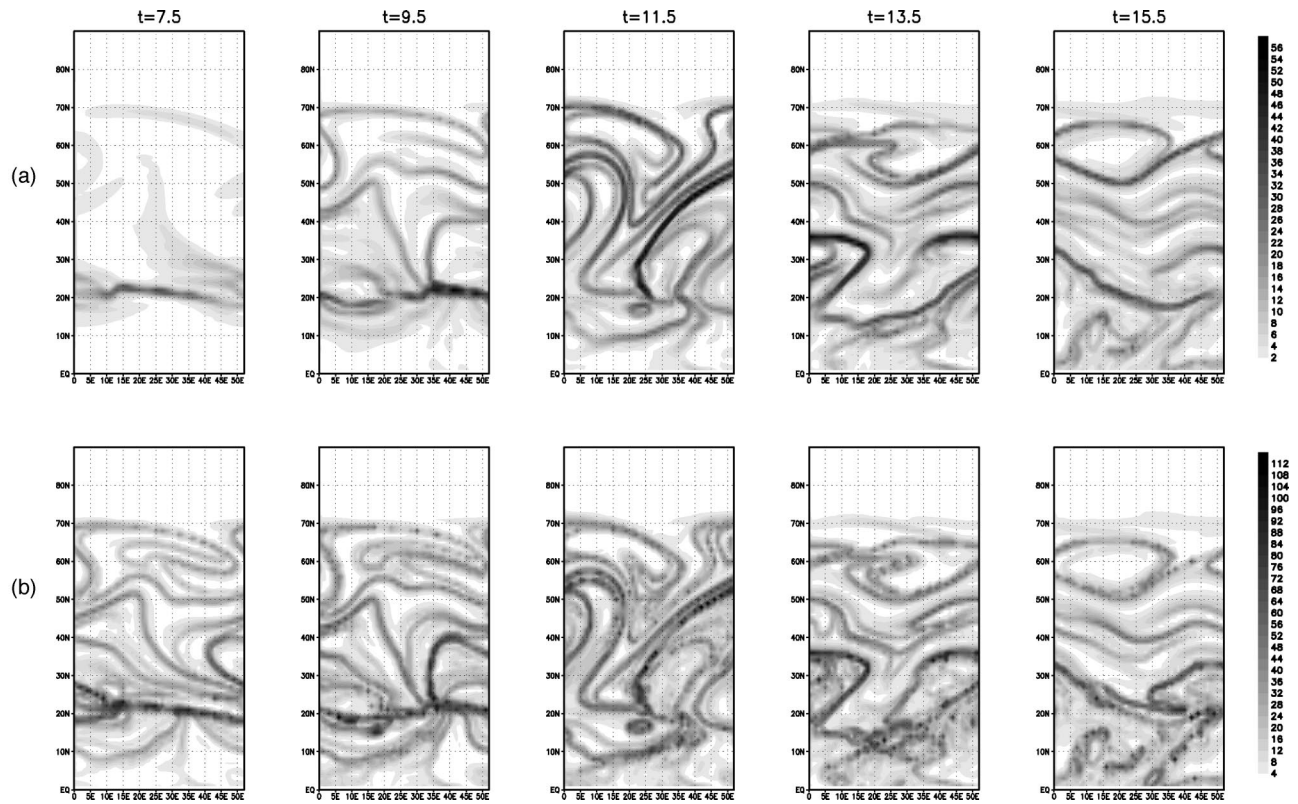


FIG. 7. Relative dispersion at different evolutionary stages of the life cycle, with seeding on the 315 K isentrope. Panels (a) show the results of five-day dispersion and panels (b) show 10 day dispersion.

the distributions are asymmetric, with a long tail for large positive values of Λ_T . As discussed by Antonsen & Ott (1989), Varosi *et al.* (1991) and Pierrehumbert & Yang (1993), the probability distribution of finite-time maximum Lyapunov exponents can provide information on the statistical properties of the gradients of concentration of a passively advected scalar field.

B. Relative dispersion

Particle pair dispersion (also called relative dispersion) provides another way of characterizing the stretching properties of fluid flows. To measure relative dispersion, we seed tracers on a regular grid with mesh size $\Delta=1^\circ$, in the Northern hemisphere between 0 and 52°E. For each particle on this grid, we distribute 8 “satellite” tracers at a radial distance of 0.25° from the central particle and we integrate the Lagrangian dynamics of this set of tracers for $T=5$ and $T=10$ days. After the time T , for each initial seeding point we calculate the average square distance between the satellite tracers and the central particle, obtaining an estimate of horizontal relative dispersion. We have explored the contribution of vertical dispersion to the total dispersion, verifying that vertical dispersion is negligible on the short time scales considered here.

Figure 7 shows relative dispersion after an integration of 5 days and 10 days, with seeding at the previously defined evolutionary stages of the life cycle, on the 315 K isentrope. By comparing these plots with the Eulerian fields depicted in Fig. 4, one sees that the “center” of the developing eddy, as

defined, e.g., by the maximum of relative vorticity, is not associated with a low value of relative dispersion, consistent with the indications provided by the Lagrangian Lyapunov exponent. The only region characterized by low relative dispersion is the cutoff region of stratospheric air that survives till the end of the life cycle. Regions of strong relative dispersion are associated with the sheared domains between the eddies and are representative of the chaotic advection taking place during a life cycle.

C. Absolute dispersion

Meridional absolute dispersion provides further characterization of the transport associated with a baroclinic life cycle. Here we define meridional dispersion for a given initial particle latitude, i.e., we use $D^2(t; y_0) = \sum_{i=1}^N (\phi_i(t) - \phi_0)^2$, where $\phi_i(t)$ is the latitude of the i th particle at time t , ϕ_0 is the initial latitude (supposed to be the same for all particles considered), and N is the number of tracers seeded at a given latitude. In this way, we obtain meridional dispersion as a function of time and the initial latitude of the tracers. Figure 8 shows the r.m.s. displacement, $D(t; \phi_0)$, as a function of the initial seeding latitude ϕ_0 , at the evolutionary times $t=9.5$, 11.5, 13.5, and 15.5 days. The maximum meridional dispersion occurs at midlatitudes, reaching its maximum during the decaying phase of the life cycle ($t=13.5$). The r.m.s. (root-mean-square) meridional displacement of tracers seeded at 70°N (well north of the initial jet, compare with Fig. 1) reaches a peak of about 25 degrees,

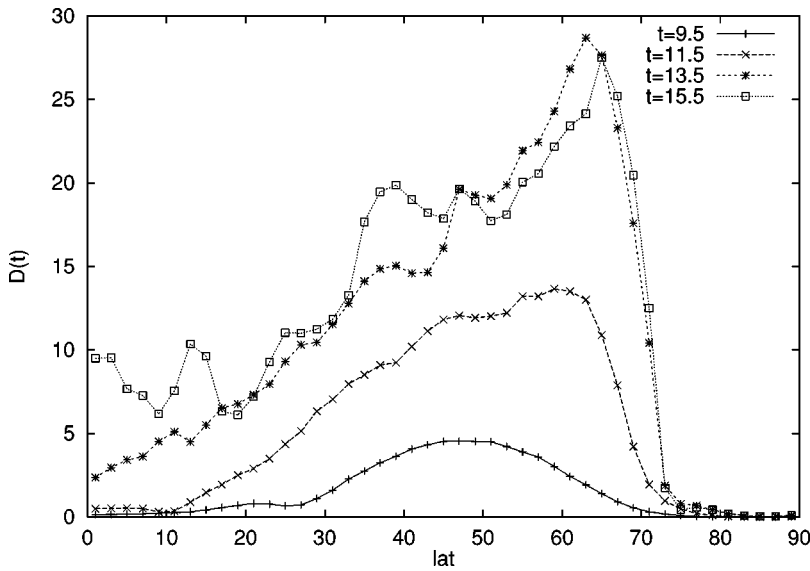


FIG. 8. Meridional r.m.s. displacement as a function of the initial tracer latitude. The different curves refer to times $t=9.5, 11.5, 13.5,$ and 15.5 days after the beginning of the life cycle.

indicating that just one single eddy life cycle is capable of inducing significant mixing across the whole midlatitudes.

VI. WHERE DOES THE FLUID COME FROM?

An important question in Lagrangian studies concerns the past history of tracers, and in particular the determination

of the initial location of a tracer particle that is found in a given position at a given time. Indeed, this issue is very important for the atmospheric moisture distribution, as fluid that comes from the tropopause level is very dry, see, e.g., Pierrehumbert & Roca (1999).

To illustrate how fluid is mixed during a baroclinic life

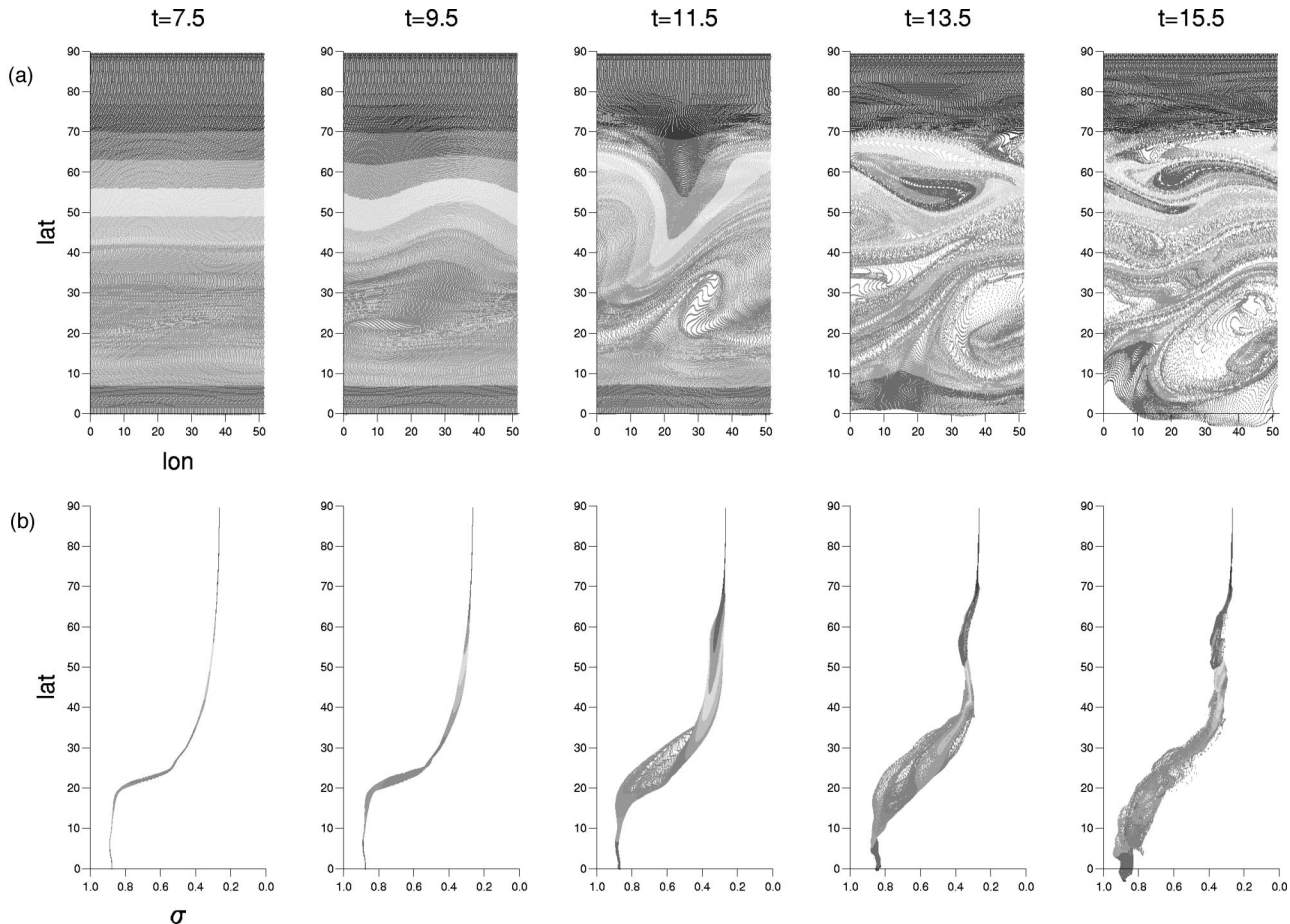


FIG. 9. Passive tracer distribution at different moments during the life cycle. Tracers are labeled according to their initial latitude. Panels (a) and (b) refer to seeding on the 315 °K isentrope and panels (c) and (d) to seeding on the 500 h Pa isobar. Panels (a) and (c) show horizontal distributions and panels (b) and (d) show vertical distributions.

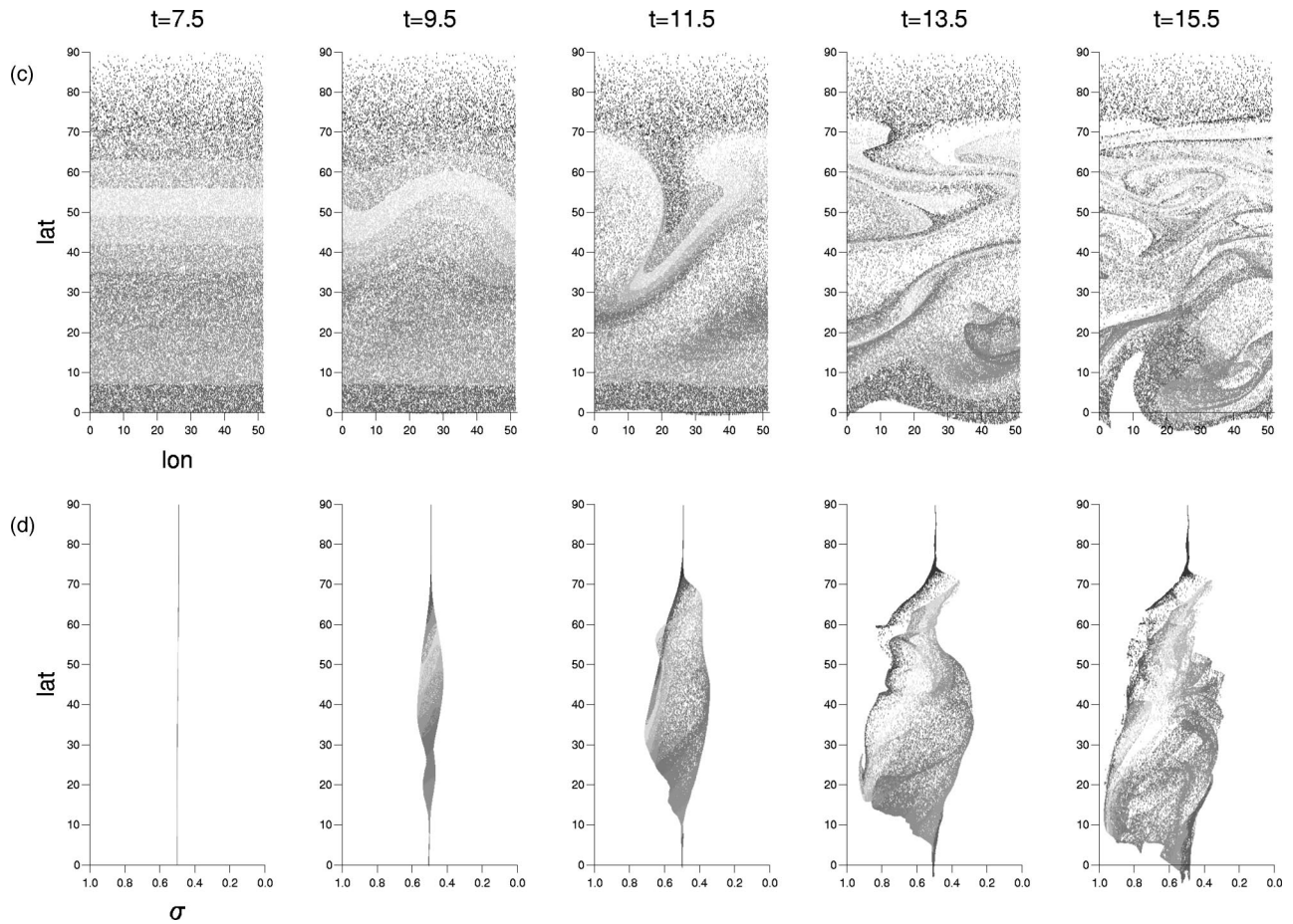


FIG. 9 (Continued.)

cycle and identify the region where a given fluid parcel has come from, we uniformly seed 74 480 tracers on the whole hemisphere, both on the 315°K isentrope and on the 500 hPa isobaric surface, and we follow the evolution of the individual tracers. Figure 9 shows the position of the tracers at the evolutionary times defined above. Each particle is gray-scale labeled according to its initial latitude. Since the Eulerian field is periodic with period $L = 360^\circ/7$ we plot tracers positions modulo L . Due to the initial zonal symmetry of the basic state, labelling with initial latitude corresponds to labelling according to the initial PV of each particle.

Figure 9 indicates the presence of strong transient horizontal mixing in the course of the life cycle. In particular, at the end of the life cycle strong meridional mixing has taken place, and a significant fraction of the fluid parcels has been transported across the jet. Note, also, that the cut-off region of stratospheric air displays very weak mixing in its interior, whereas the high shear region at its border undergoes strong mixing. This behavior is fully consistent with the results on relative dispersion and chaotic advection discussed in the previous section.

In the case of initialization on the 315°K isentrope, vertical tracer dispersion during the life cycle is relatively small, [as indicated by Fig. 9(b)], while strong vertical dispersion is present for the initialization on the 500 hPa isobar [Fig. 9(d)]. This specific behavior is due to the quasi-adiabaticity

of the life cycle studied here, which is associated with the lack of radiative and drag terms.

In order to compare mixing properties with the structure of the Eulerian field, we consider a local measure of mixing that is sensitive to the spread in the initial positions of the particles found in a given fluid region. We define a meridional mixing entropy that is low for fluid regions whose particles come from similar initial latitudes, while it achieves larger values when the fluid is well mixed and the particles come from significantly different initial latitudes. To this end, we use a measure based on the Shannon information measure [Shannon & Weaver (1949)]. To estimate it, we first divide the tracers in N_c classes according to the initial latitude. Around each gridpoint (λ, ϕ) , we define a circular neighborhood of radius r and define the density $p_i(\lambda, \phi)$ of points belonging to the class i found in this region. The entropy measure $E(\lambda, \phi) = -\sum_{i=1}^{N_c} p_i(\lambda, \phi) \log p_i(\lambda, \phi)$ then provides information on how well mixed the neighborhood (λ, ϕ) is. For a completely random distribution of initial particle positions, $p_i \approx 1/N_c$, so we use the normalized entropy $\tilde{E}(\lambda, \phi) = E(\lambda, \phi) / \log N_c$.

Figure 10 shows the normalized entropy $\tilde{E}(\lambda, \phi)$ in the case $r=2^\circ$. This measure confirms the existence of different domains with different mixing properties, and in particular provides further evidence that the cut-off air region displays

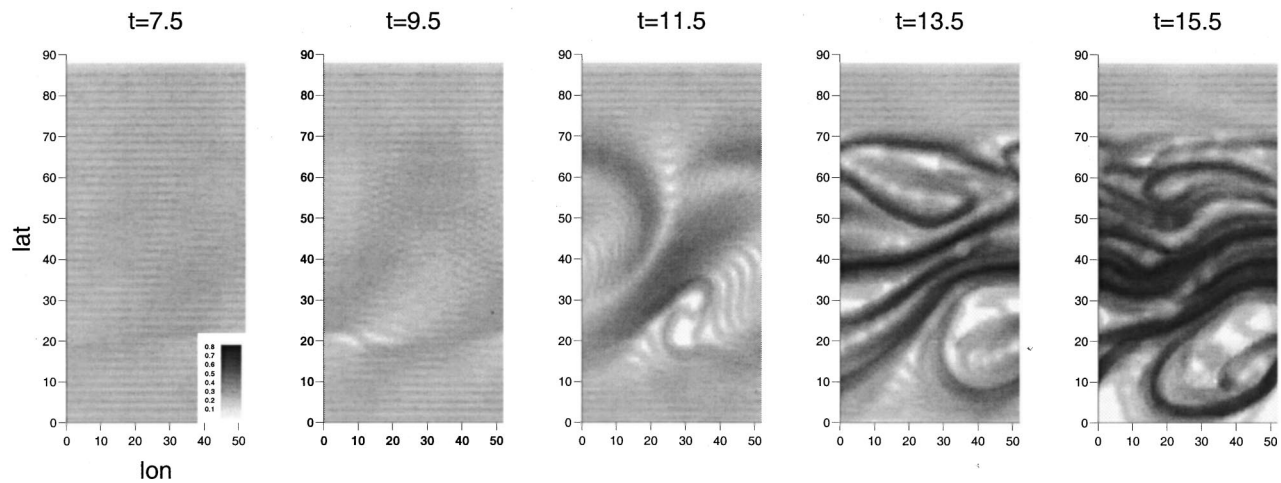


FIG. 10. Maps of the mixing entropy at different stages of the life cycle. The neighborhood size used in the calculation is $r=2^\circ$.

very low mixing in its interior and very strong mixing on its boundary. The figure also shows that mixing increases quickly during the evolution of the life cycle and it reaches its maximum during the second half of the life cycle, when the barotropic decay has already started. This agrees with the properties of tracer dispersion, that shows an increased dispersion phase during the second part of the life cycle.

VII. CONCLUSIONS

In this work we have studied the transport and mixing properties induced by a baroclinic life cycle in a mid-latitude atmosphere. We have integrated a simplified primitive equation model of the atmosphere (the PUMA SGCM) and we have followed the three-dimensional dynamics of individual Lagrangian tracers during the evolution of the life cycle. We have employed standard approaches developed in the study of two-dimensional chaotic advection, and have shown how some of these concepts can be successfully employed in the description of tropospheric transport in a dry atmosphere.

One interesting finding is that the developing cyclone does not possess closed isolines, and, opposite to quasigeostrophic vortices, it does not trap tracers. A different trapping domain does, however, exist. This is formed by a region of stratospheric cutoff, that survives for long time and behaves as a coherent vortex.

During the life cycle, strong mixing takes place outside the cutoff region. The largest stretching and mixing is found just at the edge of the cutoff region, consistent with the results obtained in the study of geostrophic turbulence. Some of the tracers disperse a long distance away from their initial position, indicating that baroclinic life cycles represent an important mechanism of stirring and mixing in mid-latitude troposphere.

The study reported here can be seen as a step toward applying the methods of chaotic advection to realistic atmospheric flows, in the spirit of Pierrehumbert & Yang (1993). The model employed here, however, is very simplified and diabatic effects are extremely limited. In particular, we do not include the direct effect of water vapor and we do not resolve the strong frontal regions that can indeed play a sig-

nificant role in tracer mixing. Future works should extend the study discussed here to more refined General Circulation Models of the atmosphere.

ACKNOWLEDGMENTS

This work has been supported by the EC contract EV5V-CT94-0503 "Variability of the North Atlantic Storm Track." J.H. acknowledges financial support by the ESF program "Transport Processes in the Atmosphere and the Oceans (TAO)."

- Antonsen, T. M. and Ott, E. (1989). "Fractal measures of passively convected vector fields and scalar gradients in chaotic fluid flows," *Phys. Rev. A* **39**, 3660–3671.
- Babiano, A., Boffetta, G., Provenzale, A., and Vulpiani, A. (1994). "Chaotic advection in point vortex models and two-dimensional turbulence," *Phys. Fluids* **6**, 2465–2474.
- Barnes, J. R. and Young, R. E. (1992). "Nonlinear baroclinic instability on a sphere: Multiple life cycles with surface drag and thermal damping," *J. Atmos. Sci.* **49**, 861–878.
- Blackburn, M. (1985). "Program description for the multilevel global spectral model." Dept. of Meteorology Univ. of Reading informal note, pp. 37.
- Bowman, K. P. and Cohen, P. J. (1997). "Interhemispheric exchange by seasonal modulation of the Hadley circulation," *J. Atmos. Sci.* **54**, 2045–2059.
- Branscome, L. E., Gutowski, W. J., Jr., and Stewart, D. A. (1989). "Effect of surface fluxes on the nonlinear development of baroclinic waves," *J. Atmos. Sci.* **46**, 460–475.
- Elmhäidi, D., Provenzale, A., and Babiano, A. (1993). "Elementary topology of two dimensional turbulence from a Lagrangian viewpoint and single particle dispersion," *J. Fluid Mech.* **257**, 533–558.
- Fraedrich, K., Kirk, E., and Lunkeit, F. (1998). "PUMA: Portable University Model of the Atmosphere." Deutsches Klimarechenzentrum, Technical Report, Vol. 16.
- Frisius, T., Lunkeit, F., Fraedrich, K., and James, I. N. (1998). "Storm-track organization and variability in a simplified atmospheric global circulation model," *Q. J. R. Meteorol. Soc.* **124**, 1019–1043.
- Gutowski, W. J., Jr., Branscome, L. E., and Stewart, D. A. (1989). "Mean flow adjustment during life cycles of baroclinic waves," *J. Atmos. Sci.* **46**, 1724–1737.
- Gutowski, W. J., Jr., Branscome, L. E., and Stewart, D. A. (1992). "Life cycles of moist baroclinic eddies," *J. Atmos. Sci.* **49**, 306–319.
- Held, I. M. and Hou, A. Y. (1980). "Nonlinear axially symmetric circulations in a nearly inviscid atmosphere," *J. Atmos. Sci.* **37**, 515–533.

- Hoskins, B. J., McIntyre, M. E., and Robertson, A. W. (1985). "On the use and significance of isentropic potential vorticity maps," *Q. J. R. Meteorol. Soc.* **111**, 877–946.
- Hoskins, B. J. and Simmons, A. J. (1975). "A multi-layer spectral model and the semi implicit method," *Q. J. R. Meteorol. Soc.* **101**, 637–655.
- James, I. N. and Dodd, J. P. (1993). "A simplified global circulation model - User's Manual," Dept. of Meteorology, Univ. of Reading Informal note, p. 42.
- James, I. N. and Gray, L. J. (1986). "Concerning the effect of surface drag on the circulation of a planetary atmosphere," *Q. J. R. Meteorol. Soc.* **112**, 1231–1250.
- Kuznetsov, L. and Zaslavsky, G. M. (1998). "Chaotic dynamics of passive particles in three-vortex systems. I. Dynamical analysis," in *Chaos, Kinetics and Nonlinear Dynamics in Fluids and Plasmas*, edited by S. Benkadda and G. M. Zaslavsky (Springer-Verlag, Berlin), pp. 119–31.
- Knobloch, E. and Weiss, J. B. (1987). "Transport by modulated traveling waves," *Phys. Rev. A* **36**, 1522–1529.
- Lee, S. and Feldstein, S. (1996). "Two types of wave breaking in an aquaplanet GCM," *J. Atmos. Sci.* **53**, 842–857.
- Lesieur, M. (1990). *Turbulence in Fluids* (Kluwer, Dordrecht), 412 pp.
- Lorenz, E. N. (1965). "A study of the predictability of a 28-variable atmospheric model," *Tellus* **17**, 321–340.
- Methven, J. and Hoskins, B. (1999). "The advection of high-resolution tracers by low-resolution winds," *J. Atmos. Sci.* **56**, 3262–3285.
- Orszag, S. A. (1970). "Transform method for calculation of vector coupled sums: Application to the spectral form of the vorticity equation," *J. Atmos. Sci.* **27**, 890–895.
- Pedlosky, J. (1987). *Geophysical Fluid Dynamics* (Springer-Verlag, Berlin).
- Pierrehumbert, R. T. (1991). "Chaotic mixing of tracer and vorticity by modulated traveling Rossby waves," *Geophys. Astrophys. Fluid Dyn.* **58**, 285–319.
- Pierrehumbert, R. T. and Yang, H. (1993). "Global Chaotic Mixing on Isoentropic Surfaces," *J. Atmos. Sci.* **50**, 2462–2480.
- Pierrehumbert, R. T. (1995). "Baroclinic instability," *Annu. Rev. Fluid Mech.* **27**, 419–467.
- Pierrehumbert, R. T. and Roca, R. (1998). "Evidence for control of Atlantic subtropical humidity by large scale advection," *Geophys. Res. Lett.* **25**, 4537–4540.
- Provenzale, A. (1999). "Transport by Coherent Barotropic Vortices," *Annu. Rev. Fluid Mech.* **31**, 55–93.
- Rhines, P. B. and Young, W. R. (1983). "How rapidly is a passive scalar mixed within closed streamlines?" *J. Fluid Mech.* **133**, 401–441.
- Robert, A. (1966). "The integration of a low order spectral form of the primitive meteorological equations," *J. Meteorol. Soc. Jpn.* **44**, 237–245.
- Shannon, C. E. and Weaver, W. (1949). *The Mathematical Theory of Communication* (University of Illinois Press, Urbana).
- Simmons, A. J. and Hoskins, B. J. (1976a). "Baroclinic Instability on the Sphere: Normal Modes of the Primitive Equations and Quasi Geostrophic Equations," *J. Atmos. Sci.* **33**, 1454–1477.
- Simmons, A. J. and Hoskins, B. J. (1976b). "Baroclinic Instability on the Sphere: Solutions with a More Realistic Tropopause," *J. Atmos. Sci.* **34**, 581–588.
- Simmons, A. J. and Hoskins, B. J. (1978). "The life cycles of some nonlinear baroclinic waves," *J. Atmos. Sci.* **35**, 414–423.
- Simmons, A. J. and Hoskins, B. J. (1980). "Barotropic influence on the growth and decay of nonlinear baroclinic waves," *J. Atmos. Sci.* **37**, 1679–1684.
- Stone, E. M., Randel, W. J., and Stanford, J. L. (1998). "Transport of passive tracers in baroclinic wave life cycles," *J. Atmos. Sci.* **56**, 1364–1381.
- Thorncroft, C. D., Hoskins, B. J., and McIntyre, M. E. (1993). "Two paradigms of baroclinic-wave life-cycle behaviour," *Q. J. R. Meteorol. Soc.* **119**, 17–55.
- Varosi, P., Antonsen, T. M., and Ott, E. (1991). "The spectrum of fractal dimensions of passively convected scaled gradients in chaotic fluid flows," *Phys. Fluids A* **3**, 1017–1028.
- Weiss, J. B., Provenzale, A., and McWilliams, J. C. (1998). "Lagrangian dynamics in high-dimensional point-vortex systems," *Phys. Fluids* **10**, 1929–1941.